IOP Publishing New J. Phys. 25 (2023) 113003 https://doi.org/10.1088/1367-2630/ad05ea

New Journal of Physics
The open access journal at the forefront of physics

Deutsche Physikalische Gesellschaft DPG
IOP Institute of Physics

Published in partnership with: Deutsche Physikalische Gesellschaft and the Institute of Physics

OPEN ACCESS

RECEIVED
8 February 2023

REVISED
14 October 2023

ACCEPTED FOR PUBLICATION
23 October 2023

PUBLISHED
3 November 2023

PAPER

Planar and tunable quantum state transfer in a splicing Y-junction Su–Schrieffer–Heeger chain

Li-Na Zheng[1], **Hong-Fu Wang**[1,2,*] **and Xuexi Yi**[1,*]

[1] Center for Quantum Sciences and School of Physics, Northeast Normal University, Changchun 130024, People's Republic of China
[2] Department of Physics, College of Science, Yanbian University, Yanji, Jilin 133002, People's Republic of China
* Authors to whom any correspondence should be addressed.

E-mail: hfwang@ybu.edu.cn and yixx@nenu.edu.cn

Keywords: quantum state transfer, quantum router, zero-energy mode, Su–Schrieffer–Heeger chain

Abstract

We present a feasible scheme to implement a planar and tunable quantum state transfer (QST) via topologically protected zero-energy mode in a splicing Y-junction Su–Schrieffer–Heeger (SSH) chain. The introduction of the elaborate nearest-neighbor (NN) hopping enables one to generate a topological interface at the central site of the Y-junction. By modulating the NN hopping adiabatically in the chain, the quantum state initially prepared at the central site can be simultaneously transferred to the three endpoints of the Y-junction with the equal/unequal probabilities. The planar distribution of QST is expected to realize a quantum router, whose function is to make the quantum information on the central site (input port) appear equally/unequally at the three endpoints (output ports) with different directions. Moreover, the numerical simulations demonstrate that the scheme possesses the robustness on the fluctuations of the NN hopping and the on-site potential in the system. Furthermore, we show that the number of the output ports with different directions can be flexibly increased in an extended X-junction SSH chain, and the experimental feasibility for implementing special QST in a superconducting qubit-resonator system is briefly discussed. Our work extends the space distribution of QST from linear distribution to planar distribution and promotes the construction of large-scale quantum networks.

1. Introduction

Quantum network [1–5], a brand-new way of information network, has attracted increasing attention since its fast processing speed, strong processing capability, and high safety. As one of the essential blocks in quantum network, the reliable quantum state transfer (QST) [6–18] between long-distance sites directly affects the accuracy and efficiency of the above procedure. Therefore, it is necessary to design and to implement a high-performance quantum communication channel. A plethora of efforts have been made to obtain the optimal channel for implementing QST, including the trapped ions [11, 12], spin chains [13–16], and nitrogen-vacancy centers [17, 18], etc. It needs to be emphasized that the intrinsic fluctuations or defects in different resources are still an unavoidable issue, which reduce the fidelity of realizing QST and inhibit the building of large-scale quantum networks.

One class of robust QST protocols come from Su–Schrieffer–Heeger (SSH) [19, 20] model of topological insulator [21, 22] have received considerable interest. They host conducting edge states, which propagate along the chain and are robust to the mild disturbances of the system [23, 24]. To this end, the topological edge states of matter have been widely applied on the establishment of quantum transfer channel. For instance, based on the superconducting Xmon qubits chain, the single-qubit state can be transferred via the topologically protected zero-energy mode [25]. With the deepening of research on topologically protected channel, different forms of SSH model [26–30] have been constructed to realize the fast and robust QST. Meanwhile, the traditional QST with only one output port has also been extended [31–33]. In reference [31],

the standard SSH model with on-site energy and next nearest-neighbor (NN) hopping can be engineered as a topological beam splitter, in which the initial state prepared at only one site can be transferred into two sites with equal probabilities. And the researchers in reference [32] have demonstrated that a topological router can be implemented in the standard SSH model with long-range hopping. These extended models dramatically enrich the content of QST and further improve the transfer efficiency. Note that the distributions of above protocols show a linear form since the state transfer between the initial state and final state is presented as a linear structure in the space. The quantum state can be transferred into one or two directions relative to the initial state. However, the quantum network is a complicated network in the practical applications, which requires quantum information to be sent and received from more different directions. Besides that, these extended protocols focus on only the equal distributions of the gap state and ignore the unequal distributions. This may limit the application of tasks related to information diversity in quantum networks. Thus the construction of the topologically protected QST channel with the realistic applications is an urgent problem.

In this paper, we propose a planar and tunable QST scheme via engineering the elaborate NN hopping in a splicing Y-junction SSH chain. We show that the elaborate NN hopping with the same hopping amplitudes as the intercell hopping added on the central site and the first site of the each SSH chain induces a special zero-energy mode, in which the zero-energy mode has the equal distributions at the three endpoints of the Y-junction. Via adiabatically ramping of the NN hopping, the initial state prepared at the central site can be transferred into the three endpoints of the Y-junction with the approximately equal probabilities. The space location among the central site and endpoints presents the planar distribution, which implies the form of QST is transformed to planar distribution. We also study that the elaborate NN hopping with different hopping amplitudes as the intercell hopping added on the central site and the first site of the each SSH chain, the zero-energy mode has the unequal distributions at the three endpoints of the Y-junction. Depending on the different elaborate NN hopping amplitudes, the probability distribution of the zero-energy mode at the three endpoints can be arbitrarily modulated. Based on the probability distribution of the zero-energy mode, we show that the planar and tunable QST channel can be constructed. If we treat the central site as the input port and treat the three endpoints as the output ports, this special topological state transfer can be naturally equivalent to a quantum router in form. Furthermore, the imperfect factors in the chain have been discussed, and the results indicate that the present protocol shows the robustness to the inevitable disorder in the NN hopping and on-site potential. Finally, we extend the current model into a splicing X-junction SSH chain, which can achieve planar QST with four different directions, and the experimental feasibility for implementing special QST is also briefly discussed.

The paper is organized as follows: in section 2, we demonstrate that a planar and tunable QST can be accomplished based on a splicing Y-junction SSH chain and reveal the robustness of the imperfect system with the disorders in NN hopping and on-site potential. In section 3, we propose an extended planar QST with four directions based on a splicing X-junction SSH chain and discuss the experimental feasibility of our protocol. Finally, a conclusion is given in section 4.

2. Planar and tunable QST assisted by the zero-energy mode

A usual QST protocol [25] in an odd-sized SSH model is based on the motion of the zero-energy edge state. By adiabatically varying the NN hopping in the chain, the zero-energy mode occupies the left or right edge with maximal distribution. Therefore, the edge state plays a role of topologically protected quantum channel to realize robust QST from the left to the right edge. The questions arise: when we design a splicing Y-junction SSH chain based on three conventional SSH chains with the same size, can each SSH chain still realize a QST? If that, can the comprehensive results of each chain realize a special QST? In the following, we show a planar and tunable state transfer channel induced by the elaborate NN hopping in a splicing Y-junction SSH chain. At the same time, we find that this special state transfer can be expected to achieve a quantum router, which provides the potential application toward topological quantum networks.

2.1. Planar QST with the equal probabilities

The universal setup of a planar QST via the topological zero-energy mode in the splicing Y-junction SSH chain is shown in figure 1. The junction contains three conventional SSH chains and a central site. For convenience, we denote the three chains by L, R, and M, according to their locations in the figure. Here, we consider cases where the three SSH chains have the same size N ($N \in$ even) and the total number is $L = 3N + 1$. When we restrict ourselves to the one-excitation subspace, the Hamiltonian of this splicing Y-junction SSH chain is written as [27, 34, 35]

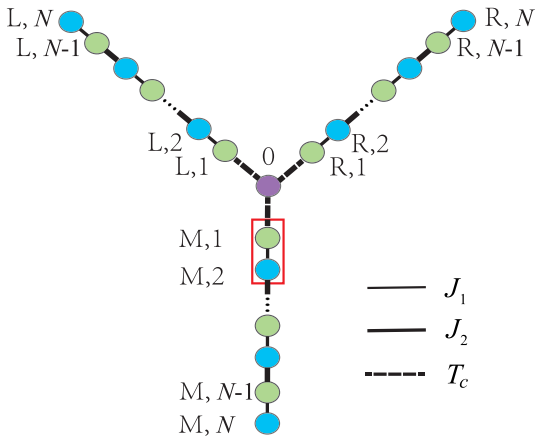

Figure 1. Schematic diagram of a splicing Y-junction SSH chain. The Y-junction consists of three conventional SSH chains and a central site. Each SSH chain with the same size N. Each color represents a class of sites. A green site and a blue site form a unit cell. The intra- and intercell couplings between two adjacent sites are J_1 and J_2. Note that the splicing Y-junction chain has the elaborate NN hopping among the each SSH chain and the central site with the hopping amplitude T_c.

$$H = J_1 \sum_{c\in C} \sum_{n_{\text{odd}=1}}^{N-1} \left(|c,n\rangle \langle c,n+1| + \text{H.c.}\right) + J_2 \sum_{c\in C} \sum_{n_{\text{even}=2}}^{N-2} \left(|c,n\rangle \langle c,n+1| + \text{H.c.}\right) + \sum_{c\in C} T_c \left(|0\rangle \langle c,1| + \text{H.c.}\right), \tag{1}$$

where $C = \{\text{L},\text{R},\text{M}\}$ is a set of positional index, and n is the site index of each SSH chain. The state localized on the nth site of the chain c is defined as $|1\rangle_{c,n}$ $(n = 1,2,\ldots,N)$ and on the central site is defined as $|1\rangle_0$. The parameters J_1 and J_2 are the NN hopping amplitudes, which are set to $J_1 = J(1+\cos\theta)$ and $J_2 = J(1-\cos\theta)$, with θ being a periodic parameter varying from 0 to 2π. In addition, the central site owns the elaborate NN hopping, which supports the NN hopping among the central site and the first site of the chain c with hopping amplitude $T_c = J_2 = J(1-\cos\theta)$.

The above Hamiltonian possesses a topological zero-energy mode in the real space energy spectrum since the system Hamiltonian respects chiral symmetry, i.e. $\hat{\Gamma}\hat{H}\hat{\Gamma}^{+} = -\hat{H}$ with $\Gamma = \text{Diag}[(-1)^0,(-1)^1,(-1)^2,\ldots,(-1)^{L-1}]$. And, the relevant wave function of zero-energy mode can be described by the following ansatz (after normalization):

$$\begin{aligned} \left|\Psi_{E=0}^{(1)}\right\rangle &= \sum_{c\in C} |0_{c,N},0_{c,N-1},\ldots,0_{c,1},1_0\rangle \ (J_1 \gg J_2), \\ \left|\Psi_{E=0}^{(2)}\right\rangle &= \frac{1}{\sqrt{3}} \sum_{c\in C} |1_{c,N},0_{c,N-1},\ldots,0_{c,1},0_0\rangle \ (J_1 \ll J_2). \end{aligned} \tag{2}$$

The analytical result indicates that the zero-energy mode occupies the central site 0 when $J_1 \gg J_2$, and concentrates toward the endpoint (c,N) when $J_1 \ll J_2$. Here, the three endpoints (L,N), (R,N), and (M,N) with the equal probabilities $1/3$ are located in different directions relative to the central site. The space distribution of the central site and the three endpoints constructs a two-dimensional plane. Obviously, the planar distribution of the zero-energy mode is totally different from the linear distribution in references [25–33].

More generally, if the central site in chain is prepared in an arbitrary state $a|0\rangle + b|1\rangle$ initially, the state of the system is written as

$$|\Psi_i\rangle = a|G\rangle + b\left|\Psi_{E=0}^{(1)}\right\rangle, \tag{3}$$

where $|G\rangle = \sum_{c\in C} |0_{c,N},0_{c,N-1},\ldots,0_{c,1},0_0\rangle$. As the NN hoppings varying from $J_1 \gg J_2$ to $J_1 \ll J_2$, the state evolves from $|\Psi_{E=0}^{(1)}\rangle$ to $|\Psi_{E=0}^{(2)}\rangle$ and $|G\rangle$ remaining unchanged. In the end, we realize the planar QST,

$$|\Psi_i\rangle = a|G\rangle + b\left|\Psi_{E=0}^{(1)}\right\rangle \rightarrow |\Psi_f\rangle = a|G\rangle + b\left|\Psi_{E=0}^{(2)}\right\rangle. \tag{4}$$

The information of the central site $a|0\rangle + b|1\rangle$ was transferred to the three endpoints. For the sake of simplicity, we take the transfer of $|\Psi_{E=0}^{(1)}\rangle \rightarrow |\Psi_{E=0}^{(2)}\rangle$ as example in the following numerical analysis and discussion.

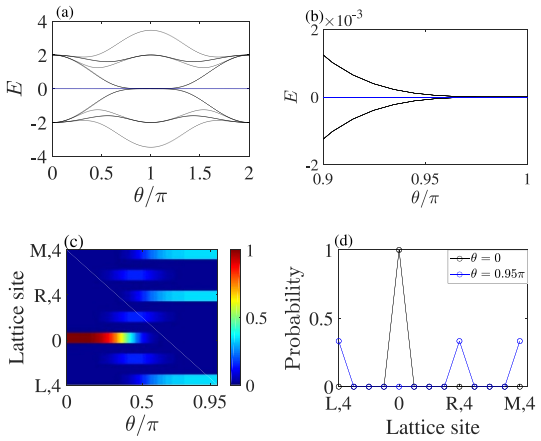

Figure 2. (a) Energy spectrum of the splicing Y-junction SSH chain versus the parameter θ. The gap state with zero energy is pinned in the energy gap. (b) Enlargement of the energy spectrum in the region of $\theta \in [0.9\pi, \pi]$. (c) Distribution of the zero-energy mode versus the parameter θ. ($\theta \in [0, 0.95\pi]$) (d) Probability amplitude of the zero-energy mode when $\theta = 0$ or $\theta = 0.95\pi$. The size of the chain is $L = 3N + 1 = 13$. Here, we take $J = 1$ as the energy unit.

To certify the above claims, we plot the energy spectrum of the system and the distribution of the zero-energy mode when the size of each SSH chain is $N = 4$, as shown in figure 2. Notably, we choose $L = 3N + 1 = 13$ as an example throughout the paper without special emphasis. We find that each eigenvalue E accompanied by a chiral symmetric partner with eigenvalue $-E$ and the eigenvalue $E = 0$ is pinned in the whole energy gap. When θ gradually increases to π, the zero-energy mode almost touches the bulk state, as shown in figure 2(a). It is worth emphasizing that the zero-energy mode is nondegenerate in the parameter space $0.9\pi < \theta < 0.95\pi$ in figure 2(b). In order to avoid the disturbance of the bulk state to the zero-energy mode, we choose the distribution of the zero-energy mode for the appointed parameter range with $\theta \in [0, 0.95\pi]$. As shown in figure 2(c), the zero-energy mode occupies the central site 0 when $\theta \in [0, 0.5\pi]$ and concentrates toward the three endpoints (L, N), (R, N), and (M, N) when $\theta \in [0.5\pi, 0.95\pi]$. Further, we plot the detailed distribution of the zero-energy mode with the specific parameters $\theta = 0$ and $\theta = 0.95\pi$ in figure 2(d). It can be found that the zero-energy mode has probability 1 at the central site 0 and the equal probabilities 1/3 at the three endpoints (L, N), (R, N), and (M, N). Obviously, these numerical simulation results are in good agreement with the theoretical analysis in equation (2).

The root reason of the zero-energy mode with a planar distribution is that, when $\theta \in [0, 0.5\pi]$, the strong hopping amplitude J_1 and the weak hopping amplitude $J_2 = T_c$ lead each SSH chain to be split into several dimers and the central site to be isolated. In this way, the zero-energy mode mainly occupies the central site and the central site becomes the topological edge state, as shown in figure 3(a). On the contrary, when $\theta \in [0.5\pi, 0.95\pi]$, the NN hopping amplitude and the elaborate NN hopping amplitude satisfy $J_2 = T_c > J_1$, indicating that the last site of each SSH chain is isolated. Then, the zero-energy mode occupies the three endpoints (L, N), (R, N), and (M, N) and the three endpoints become the special edge states. Furthermore, each SSH chain connects the central site with the same elaborate NN hopping amplitude T_c. This signifies that each SSH chain occupies the equal weight for the central site and the probability distributions of zero-energy mode in the three endpoints are equal. The particular distribution predicts that the zero-energy state may experience the planar transfer from the central site to the three endpoints of the Y-junction with different directions when the periodic parameter θ varies from 0 to 0.95π.

The special QST between $|\Psi^{(1)}_{E=0}\rangle$ and $|\Psi^{(2)}_{E=0}\rangle$ can be realized via the evolution of the time-dependent Hamiltonian. We rewrite the periodic parameter θ as the time-dependent version $\theta = \Omega t$ with the ramping speed Ω and the time t. If the system is driven sufficiently slowly during the transfer process, we can guarantee the zero-energy eigenstate without exciting other eigenstates. Therefore, it is necessary to evaluate the appropriate adiabatic parameter Ω and ensure the evolution process against the influence of the bulk state. In figure 4, we simulate the QST fidelity as a function of the ramping speed Ω for different sizes of the splicing Y-junction SSH chain. The fidelity in our work can be defined as $F = |\langle\Psi^{(2)}_{E=0}|\psi_{\mathrm{end}}\rangle|^2$, where $|\psi_{\mathrm{end}}\rangle$ denotes the evolved final state and $|\Psi^{(2)}_{E=0}\rangle$ represents the ideal final state of the planar QST. The results show that the range of the appropriate adiabatic parameter Ω is increased since the size of a splicing Y-junction SSH chain decreases. For instance, the shorter chain $L = 13$ with $F \approx 1$ requires $\Omega \leqslant 0.075$. For a longer chain $L = 25$, the high fidelity $F \approx 1$ occurs for $\Omega \leqslant 0.023$. Figure 4 reveals the prefect QST can be realized when the system with different sizes satisfies the reasonable adiabatic condition.

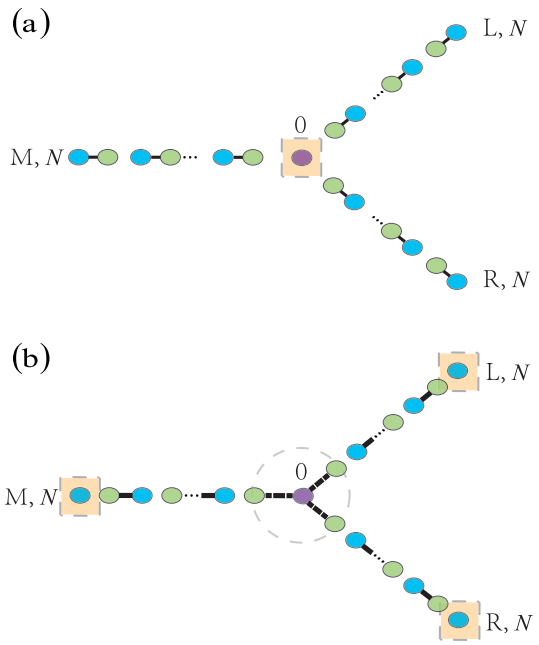

Figure 3. The analysis of the distribution for the zero-energy mode when $\theta \in [0, 0.95\pi]$. (a) When $\theta \in [0, 0.5\pi]$, the strong hopping amplitude J_1 and the weak hopping amplitude $J_2(T_c)$ lead that the central site 0 becomes an isolated site. As a result, the zero-energy mode is localized at the central site. (b) When $\theta \in [0.5\pi, 0.95\pi]$, the strong hopping amplitude $J_2(T_c)$ and the weak hopping amplitude J_1 lead that the endpoint (c, N) becomes an isolated site. As a result, the zero-energy mode is localized at the endpoint (c, N). (The isolated site is filled in the orange shading.)

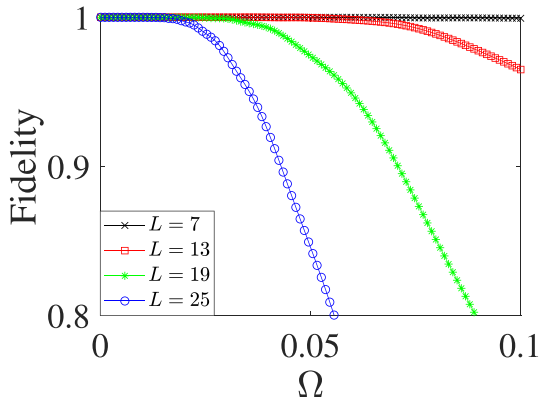

Figure 4. The fidelity of the planar transfer versus the ramping speed Ω corresponds to different size of the splicing Y-junction SSH chain. Here, we take $J = 1$ as the energy unit.

In practice, the precise control of a tunable coupling parameter is impossible during experimental implementation. Therefore, it is necessary to evaluate the robustness of the planar QST when the fluctuation exists in the tunable coupling (J_1, J_2 and T_c). This imperfection can be described by the Hamiltonian

$$H_{\mathrm{ND}} = (J_1 + W\delta)\sum_{c\in C}\sum_{n_{\mathrm{odd}}=1}^{N-1}(|c,n\rangle\langle c,n+1| + \mathrm{H.c.}) + (J_2 + W\delta)\sum_{c\in C}\sum_{n_{\mathrm{even}}=2}^{N-2}(|c,n\rangle\langle c,n+1| + \mathrm{H.c.}) + \sum_{c\in C}(T_c + W\delta)(|0\rangle\langle c,1| + \mathrm{H.c.}), \quad (5)$$

where W represents the strength of the random disorder in NN hopping and δ is a random number in the range of $[-0.5, 0.5]$. For each $W\delta$, we choose 101 samples to perform the numerical simulation throughout this work. In figure 5(a), we plot fidelity of the QST to weigh its resilience of the NN disorder in different sizes. Here, we choose the ramping speed $\Omega = 0.001$ to realize the adiabatic evolution process, which obeys the adiabatic condition of the size L ($L = 7, 13, 19, 25$) in figure 4. The numerical results show that, corresponding to the mild enough disorder strength $\log_{10}(W) \in [-2, -0.75]$, the state transfer between

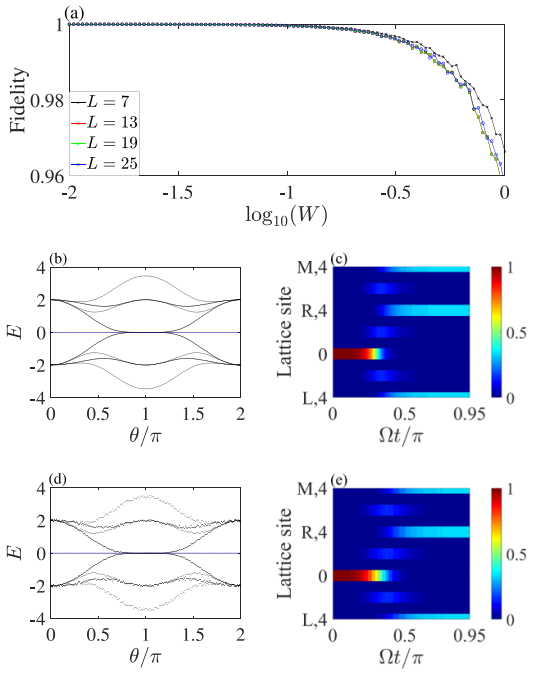

Figure 5. (a) The fidelity of the planar QST against the strength of the NN disorder corresponds to different sizes of the splicing Y-junction SSH chain. (b) The energy spectrum of the imperfect system with the NN disorder strength $W = 0.01$. (c) The related state transfer via the evolution of zero-energy mode in the figure 5(b), where the adiabatic parameter satisfies $\Omega = 0.001$. (d) The energy spectrum of the imperfect system with the NN disorder strength $W = 0.1$. (e) The related state transfer via the evolution of zero-energy mode in the figure 5(d), where the adiabatic parameter satisfies $\Omega = 0.001$. The size of the splicing Y-junction SSH chain in figures 5(b)–(e) is $L = 3N + 1 = 13$. Here, we take $J = 1$ as the energy unit.

$|\Psi^{(1)}_{E=0}\rangle$ and $|\Psi^{(2)}_{E=0}\rangle$ can be realized with a high enough fidelity $F \approx 1$. This indicates that the present protocol is naturally immune to the mild disorder in NN hopping with the size L ($L = 7, 13, 19, 25$). To explore the reason of the imperfect NN hopping has barely effect on the QST, we numerically simulate the energy spectrum and state evolution with different disorder strength $\log_{10}(W)$ for the size $L = 13$. For the slow enough ramping speed $\Omega = 0.001$ and mild enough disorder strength $\log_{10}(W) = -2$, it is straightforward to observe that the gap state with zero energy exists stably in the energy spectrum and the bulk state occurs a slight fluctuation, as shown in figure 5(b). Considering the above zero-energy mode corresponds to a planar transfer channel, the QST between the state $|\Psi^{(1)}_{E=0}\rangle$ and $|\Psi^{(2)}_{E=0}\rangle$ can be realized when the mild disorder is added into the NN hopping. This is verified by our numerical simulation in figure 5(c). When the mild enough disorder strength $\log_{10}(W)$ increases, the bulk state produces a larger fluctuation. However, the gap state still keep the zero energy, as shown in figure 5(d). In this way, the QST can be successfully implemented based on the gap state, as shown in figure 5(e). Figure 5 demonstrates that nearly perfect QST can be achieved when the mild NN disorder added on the system.

In addition, the on-site potential of site may possess the disorder due to the modulation of external control, namely, on-site disorder. Then, the splicing Y-junction chain can be described as,

$$H_{\mathrm{OD}} = \sum_{c\in C}\sum_{n=1}^{N} V\delta\,|c,n\rangle\langle c,n| + V\delta\,|0\rangle\langle 0| + J_1\sum_{c\in C}\sum_{n_{\mathrm{odd}}=1}^{N-1}\left(|c,n\rangle\langle c,n+1| + \mathrm{H.c.}\right) + J_2\sum_{c\in C}\sum_{n_{\mathrm{even}}=2}^{N-2}\left(|c,n\rangle\langle c,n+1| + \mathrm{H.c.}\right) + \sum_{c\in C} T_c\left(|0\rangle\langle c,1| + \mathrm{H.c.}\right), \tag{6}$$

where the term $V\delta\,|c,n\rangle\langle c,n|$ ($V\delta\,|0\rangle\langle 0|$) represents the on-site disorder added on the site (c,n) [central site 0] with the disorder strength V. Here, we mainly consider two cases of on-site disorder: one where the on-site disorders are imposed on all sites (disorder 1) and another where the on-site disorders are added on the sectional sites (disorder 2) [the central and three endpoints are exempted]. From the figure 6, we investigate that the disorder 2 is almost has no influence on the QST with a high fidelity $F \approx 1$. When the on-site disorder are respectively added on all sites, we observe that the disorders have little effect on the planar QST with respect to $\log_{10}(V) < -1.8$ while the fidelities show a rapid trend of decline with $\log_{10}(V) > -1.8$. In the case of disorder 2, the protocol proves to be even more robust than the case in disorder 1. The reason is that the planar QST mainly occupies the site (c, N) and central site 0. Figure 6

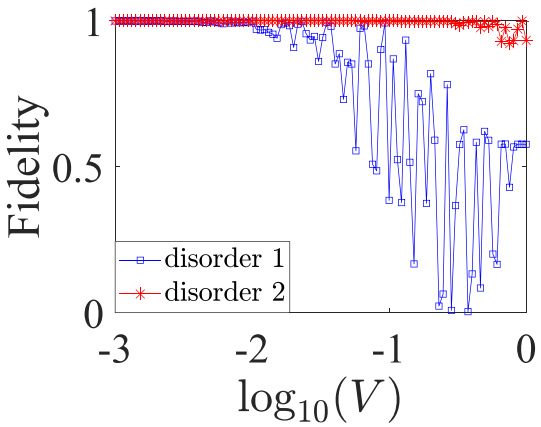

Figure 6. The fidelity of the planar QST with equal probabilities against the strength of the on-site disorder. The size of the chain is $L = 3N + 1 = 13$ and the ramping speed Ω satisfies $\Omega = 0.001$. Here, we take $J = 1$ as the energy unit.

reveals the on-site disorder added on the site (c, n) $(n \neq N)$ has minimal effect of the planar QST and our protocol is insensitive to the mild disorder in on-site potential.

Based on the matrix representation of the Hamiltonian the disorder on the NN hopping is commonly addressed as off-diagonal disorder, while the disorder on the on-site potential of site is addressed as diagonal disorder. The off-diagonal disorder keeps chiral symmetry and the zero-energy mode is insensitive to the mild disorder in the NN hopping. And, for the special distribution of the zero-energy mode, the diagonal disorder in the special site (c, n) $(n = 1, 2, 3, \ldots, N-1)$ has barely effect on the QST. To sum up, benefiting from the protection of the energy gap and the distribution of the zero-energy mode, the QST with equal probabilities in the splicing Y-junction SSH chain is naturally immune to the mild disorder of the NN hopping and the on-site potential.

The above process is a kind of special topological QST in SSH model, in which the quantum state initially prepared at the central site (regarded as input port) can be equally transferred toward the three endpoints (regarded as output ports). We here have two remarks. First, compared to the traditional topological QST with only one output port, the present protocol can realize the QST with multiple output ports. In the quantum network, efficiency and scalability are the basis of the large-scale quantum information processing. Second, the space distribution among the central site and the three endpoints is a planar structure, which extends the QST form from linear distribution to planar distribution. The quantum state can be sent with more different directions. Thus, the appearance of a planar QST with multiple output ports will greatly supply the applications of the topological matters in large-scale quantum network.

2.2. Planar QST with the unequal probabilities

We have implemented a planar QST with the equal probabilities in a splicing Y-junction SSH chain. The reason of the equal probabilities in the three endpoints is that, the same NN hopping amplitudes T_c lead each SSH chain to hold the equal weight for the central site. In this way, the quantum state initially prepared at the central site can be pumped toward the three endpoints with the equal probabilities. Following the essence of the equal probabilities in the three endpoints, we adjust the hopping amplitudes of the elaborate NN hopping T_c, in which the NN hopping T_c satisfies T_{L}:T_{R}:$T_{\mathrm{M}} = 1$:0.5:0.5. For different NN hopping amplitudes T_c, each SSH chain occupies the unequal weight for the central site. Accordingly, the probability distributions of the zero-energy mode in the three endpoints are unequal. To sustain our claim, we make a related numerical simulation. Similar to the case of the elaborate NN hopping amplitudes satisfy T_{L}:T_{R}:$T_{\mathrm{M}} = 1$:1:1, the present energy spectrum also possesses a zero-energy mode, as shown in figure 7(a). Obviously, the system follows chiral symmetry due to different NN hopping amplitudes T_c as the off-diagonal terms. The zero-energy mode is independent when the periodic parameter satisfies $\theta \in [0, 0.95\pi]$ in figure 7(b). In order to demonstrate that different NN hopping amplitudes T_c steer the zero-energy mode to occupy the three endpoints with unequal probabilities, we plot the distribution of the zero-energy mode in figure 7(c). We can conclude that the zero-energy mode is localized at the central site 0 within $\theta \in [0, 0.5\pi]$ while it is unequally distributed at three endpoints (L, N), (R, N), and (M, N) within $\theta \in [0.5\pi, 0.95\pi]$. To make the distribution of the zero-energy mode more accurately, we plot probability distribution of the zero-energy mode. As shown in figure 7(d), the zero-energy mode possesses equal probabilities 1/6 at the endpoints (R, N) and (M, N) while at the endpoint (L, N) possesses 4/6. In this way, it is easy to infer that the initial state $|\Psi_{E=0}^{(1)}\rangle$ can be transferred into the three endpoints with unequal probabilities.

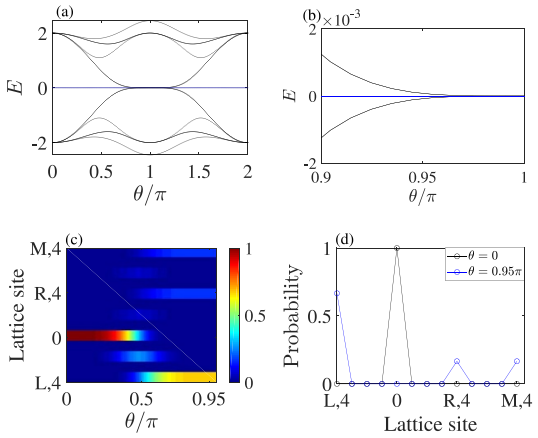

Figure 7. (a) Energy spectrum of the splicing Y-junction SSH chain versus the parameter θ. The gap state with zero energy is pinned in the energy gap. (b) Enlargement of the energy spectrum in the region of $\theta \in [0.9\pi, \pi]$. (c) Distribution of the zero-energy mode versus the parameter θ. ($\theta \in [0, 0.95\pi]$) (d) Probability amplitude of the zero-energy mode when $\theta = 0$ or $\theta = 0.95\pi$. The size of the chain is $L = 3N + 1 = 13$. Here, we take $J = 1$ as the energy unit.

Next, by modulating the elaborate NN hopping amplitudes T_c, we can engineer a series of the planar QST channels based on the unequal distribution of the zero-energy mode. Figure 8 shows multiple QST with unequal probabilities when the system possesses different NN hopping amplitudes T_c. In figure 8(a), the NN hopping amplitudes T_c satisfy $T_{\rm L} : T_{\rm R} : T_{\rm M} = 1 : 0 : 0$, indicating that two SSH chains have no coupling with the central site and the initial state on the central site only can be transferred into the endpoint $({\rm L}, N)$. Namely, the present form of the splicing Y-junction SSH chain is equivalent to a conventional odd-sized SSH chain, which realize a linear QST from the central site 0 to the endpoint $({\rm L}, N)$. Subsequently, we plot a series of the state transfer process of the initial state $|\Psi^{(1)}_{E=0}\rangle$ with different NN hopping amplitudes T_c. The initial state at the central site can be transferred to the evolved final state with the unequal probability at three endpoints $({\rm L}, N)$, $({\rm R}, N)$, and $({\rm M}, N)$ in figures 8(b)–(f). It is evident that a planar and tunable QST can be implemented.

Similarly, to test the robustness of the tunable QST, we study the effects of different type of disorder in figure 9. First, we plot the disorder of the NN hopping versus the different NN amplitudes T_c on the fidelity, as shown in figure 9(a). The numerical results reveal that, corresponding to the small enough ramping speed $\Omega = 0.001$ and different NN hopping amplitudes T_c, the mild parameter W with $\log_{10}(W) < -1.3$ ensures that the almost perfect state transfer can be realized with a high enough fidelity $F \approx 1$ for the chain size $L = 3N + 1 = 13$. The on-site disorders added on all sites also has been discussed in figure 9(b). The numerical results reveal conclusions similar to the cases in figure 6. The robustness of the protocol to the disorder and perturbation provides much more convenience for the experimental realization and the practical application.

In section 2.2, by varying the elaborate NN hopping amplitudes T_c flexibly, the special channel is engineered to implement the planar and tunable QST in a splicing Y-junction SSH chain. The present scheme extends the transfer structure from linear distribution to planar distribution and realizes the tunable probabilities at the three endpoints of a Y-junction. The extraordinary performance indicates that, from the perspective of treating the central site as the input port and treating the three endpoints of the Y-junction as output ports, the present state transfer is thus equivalent to a quantum router [36–43] and naturally immune to the mild local perturbation. The thickness of the black line represents the quantum state prepared at input port can be transferred into three output ports with different probabilities, as shown in figure 10. The appearance of the quantum router with planar and tunable output ports will greatly supply the applications of the topological matters in large-scale quantum network with much more universal and flexible.

3. Extension and implementation

In the above, we have demonstrated that a planar and tunable QST protocol for transferring the quantum state from the central site to the three endpoints with different directions through a splicing Y-junction SSH chain. Here, we will extend a Y-junction SSH chain into a X-junction SSH chain and further advance the process of a planar QST. Based on the Y-junction SSH chain, an additional SSH chain is introduced in figure 11, which also connects with the central site by the NN hopping T_c, namely, a splicing X-junction SSH chain. Similarly, we plot the energy spectrum as shown in figure 12(a), the zero-energy mode is pinned in the

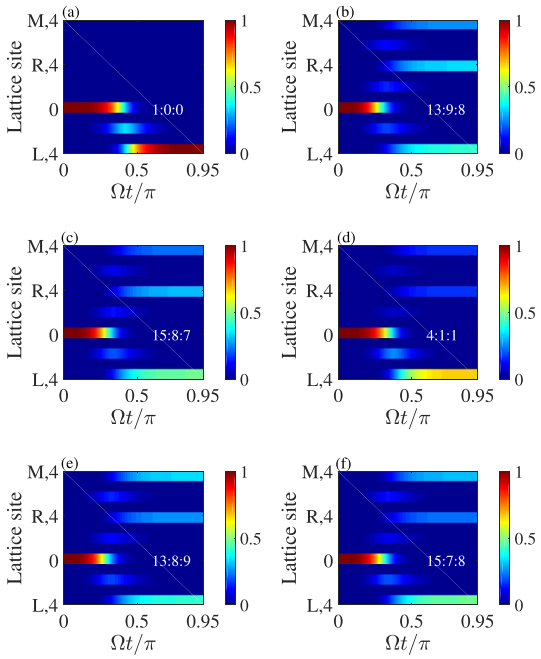

Figure 8. The evolution of the initial state $|\Psi^{(1)}_{E=0}\rangle$ when a splicing Y-junction SSH chain possesses the unequal NN hopping amplitudes T_c. (a) T_L:T_R:T_M = 1:0:0. Probability distribution of the evolved final state satisfies $P_{L,N}$:$P_{R,N}$:$P_{M,N}$ = 1:0:0 (b) T_L:T_R:T_M = 1:0.9:0.8. Probability distribution of the evolved final state satisfies $P_{L,N}$:$P_{R,N}$:$P_{M,N}$ = 13:9:8. (c) T_L:T_R:T_M = 1:0.8:0.7. Probability distribution of the evolved final state satisfies $P_{L,N}$:$P_{R,N}$:$P_{M,N}$ = 15:8:7. (d) T_L:T_R:T_M = 1:0.5:0.5. Probability distribution of the evolved final state satisfies $P_{L,N}$:$P_{R,N}$:$P_{M,N}$ = 4:1:1. (e) T_L:T_R:T_M = 1:0.8:0.9. Probability distribution of the evolved final state satisfies $P_{L,N}$:$P_{R,N}$:$P_{M,N}$ = 13:8:9. (f) T_L:T_R:T_M = 1:0.7:0.8. Probability distribution of the evolved final state satisfies $P_{L,N}$:$P_{R,N}$:$P_{M,N}$ = 15:7:8. The size of the chain is $L = 3N + 1 = 13$ and the ramping speed Ω satisfies $\Omega = 0.001$. Here, we take $J = 1$ as the energy unit.

energy gap. The figure 12(b) shows the magnified spectrum of the system in the special parameter range of $\theta \in [0.9\pi, \pi]$ and the zero-energy mode is not contact with the bulk state. Therefore, the zero-energy mode is indeed independent of the bulk state for the parameter satisfies $\theta \in [0, 0.95\pi]$. In order to prove that the extended model can realize a planar QST with more directions, we give the corresponding zero-energy mode distribution for the parameters $\theta = 0$ and $\theta = 0.95\pi$ in figure 12(c). It is shown that the zero-energy mode is mainly localized at the central site 0 with $\theta = 0$ while it is uniformly distributed at four endpoints of the X-junction with $\theta = 0.95\pi$. The simulation reveals that the zero-energy mode in a splicing X-junction SSH chain can be treated as the topological channel to implement the multiple directions QST. The relevant evolution process is shown in figure 12(d) and the numerical results clearly show that the information encoded on the central site 0 can be transferred to the site (c', N) [(L1, N), (L2, N), (R1, N), (R2, N)] via the adiabatic pumping of the zero-energy state. Obviously, when the splicing SSH chain possesses the multiple SSH chains, a series of similar planar QST channels with multiple directions can be designed. The above extended model greatly facilitates the process of the planar QST and provides the basis for large-scale quantum network construction.

In principle, our state transfer scheme can be applicable to any kinds of superconducting systems [25, 44–48]: qubit chains, qubit-resonator chains, and resonator chains. Here, we manage to realize such a scheme in a superconducting qubit-resonator chain. The feasibility of the scheme comes from the precise modulation of the coupling (NN hopping) between sites (qubit and resonator) in a splicing Y-junction (X-junction) SSH chain. For superconducting qubit-resonator chain, two adjacent sites (qubit and resonator) can be dynamically tuned by a coupler of superconducting quantum interference device (SQUID), as shown in figure 13. Utilizing the controlled voltage pulses of a waveform generator to tune the flux threading the SQUID loop [49, 50], the NN hopping between qubit and resonator can be modulated arbitrarily. The typical coupling between two superconducting elements can be tuned in the range of $1 \sim 50$ MHz [51], which provides a considerably wide tuning range for the amplitudes of the NN hopping. Our scheme is not limited to the superconducting qubit-resonator chain, and can also be applied to other types of superconducting element. The similar superconducting systems of the SSH model with different forms have also been demonstrated [25, 27, 29, 35]. Besides, with a typical coupling strength of $J/2\pi = 50$ MHz and the ramping speed $\Omega = 0.001$, the operation time can be achieved in $T_{L=13} = 0.95\pi/\Omega \approx 9.5\,\mu$s. Under the current experimental conditions, the decoherence time of the

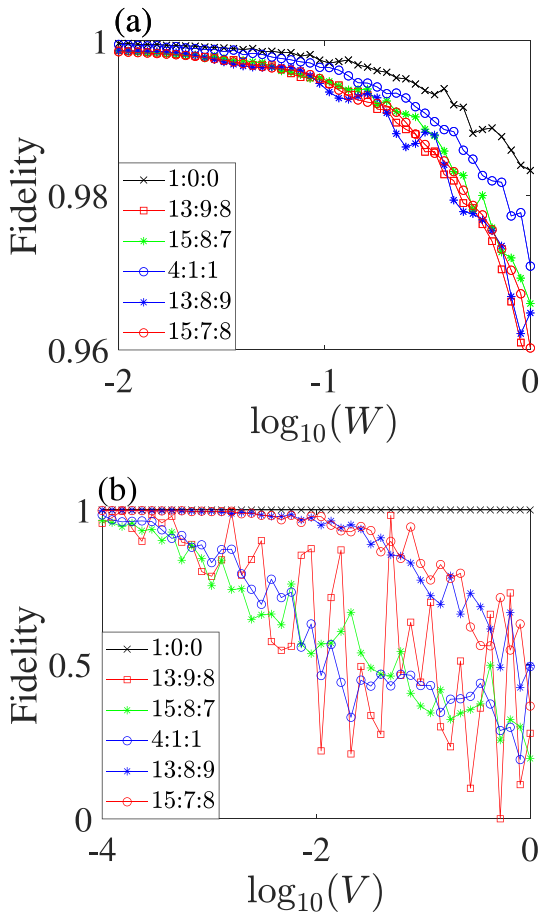

Figure 9. (a) The fidelity of the planar QST against the strength of the NN disorder corresponds to the unequal NN hopping amplitudes T_c of a splicing Y-junction SSH chain. (b) The fidelity of the planar QST against the strength of the on-site disorder corresponds to the unequal NN hopping amplitudes T_c of a splicing Y-junction SSH chain. The size of the chain is $L = 3N + 1 = 13$ and the ramping speed Ω satisfies $\Omega = 0.001$. Here, we take $J = 1$ as the energy unit.

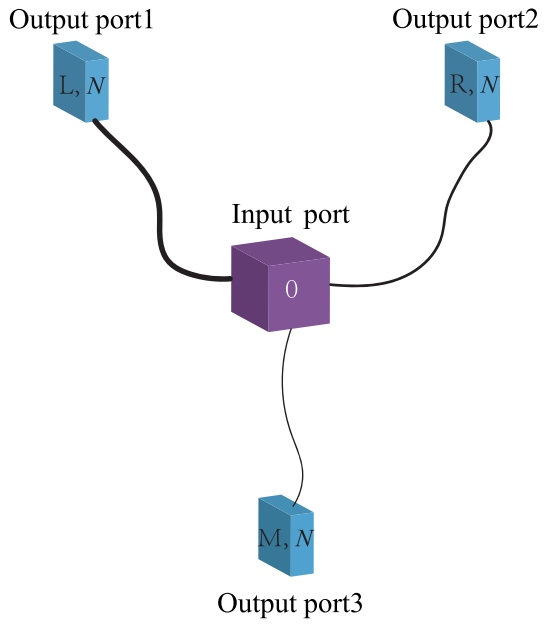

Figure 10. The function of the present scheme, in which the central site is treated as the input port and the endpoint (c, N) is treated as the output port. The present process of the state transfer is naturally equivalent to a quantum router in form.

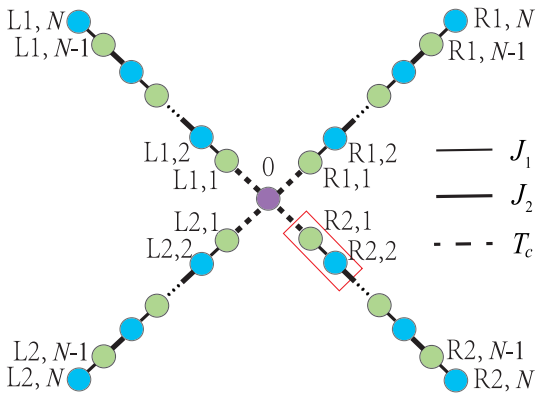

Figure 11. Schematic diagram of a splicing X-junction SSH chain. The X-junction consists of four conventional SSH chains and a central site. Each SSH chain with the same size N. Each color represents a class of sites. A green site and a blue site form a unit cell. The intra- and intercell couplings between two adjacent sites are J and J. Note that the X-junction chain has the elaborate NN hopping among the each chain and the central site with the same hopping amplitude T_c.

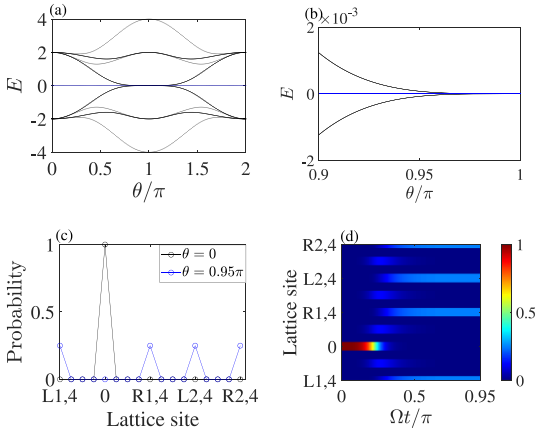

Figure 12. (a) Energy spectrum of the splicing X-junction SSH chain versus the parameter θ. The gap state with zero energy is pinned in the energy gap. (b) Enlargement of the energy spectrum in the region of $\theta \in [0.9\pi, \pi]$. (c) Probability amplitude of the zero-energy mode when $\theta = 0$ or $\theta = 0.95\pi$. (d) The evolution of the initial state $|\Psi^{(1)}_{E=0}\rangle$ when the splicing X-junction SSH chain possesses the equal NN hopping amplitudes T_c. The size of the chain is $L = 4N + 1 = 17$ and the ramping speed Ω satisfies $\Omega = 0.001$. Here, we take $J = 1$ as the energy unit.

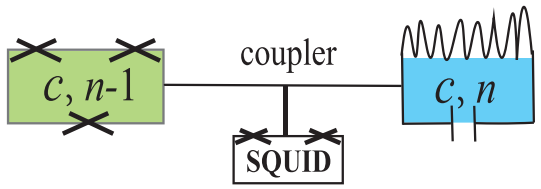

Figure 13. Circuit schematic of one unit cell in superconducting qubit-resonator chain. The coupling strength can be dynamically tuned by a coupler of SQUID.

superconducting magnetic flux qubit can be achieved on 1 ms [52] and the superconducting resonator lifetimes can be achieved between 1 and 10 ms [53, 54], which are far more than the evolution time $T_{L=13}$. Therefore, based on the current technique of superconducting system, our scheme is entirely possible. In addition, the splicing Y-junction structure in minimum control also can implement the present scheme, which is contributed to reducing the difficulty of experimental operation.

4. Conclusions

In conclusion, we have proposed a planar and tunable QST scheme for transferring the quantum state from the central site to the three endpoints with different directions through a splicing Y-junction SSH chain. The

elaborate NN hopping amplitudes induce the zero-energy mode to occupy the three endpoints of the Y-junction with equal/unequal probabilities, which makes the present topological channel have many potential applications in quantum router device. Moreover, we study the influence of fluctuation or disturbance in the NN coupling or on-site potential on the present scheme. The simulation results demonstrate that the proposed scheme is naturally immune to the mild NN disorder and on-site disorder of the splicing Y-junction SSH chain. Our scheme can also be extended to realize a planar QST with four different directions in a splicing X-junction SSH chain. Furthermore, we also give the experimental implementation of the present scheme by using superconducting qubit-resonator system (a splicing Y-junction or X-junction SSH chain). Our work opens up a new path for the implementation of a planar and tunable QST and further promotes the building of large-scale quantum networks.

Data availability statement

All data that support the findings of this study are included within the article (and any supplementary files).

Acknowledgment

This work was supported by the National Natural Science Foundation of China under Grant Nos. 12375020, 12074330, and 12175033.

ORCID iD

Hong-Fu Wang https://orcid.org/0000-0002-6778-6330

References

[1] Yurke B and Denker J S 1984 Quantum network theory *Phys. Rev.* A **29** 1419
[2] Elliott C 2002 Building the quantum network *New J. Phys.* **4** 46
[3] Kimble H J 2008 The quantum internet *Nature* **453** 1023
[4] Simon C 2017 Towards a global quantum network *Nat. Photon.* **11** 678
[5] Pompili M *et al* 2021 Realization of a multinode quantum network of remote solid-state qubits *Science* **372** 6539
[6] Cirac J I, Zoller P, Kimble H J and Mabuchi H 1997 Quantum state transfer and entanglement distribution among distant nodes in a quantum network *Phys. Rev. Lett.* **78** 3221
[7] Van Enk S J, Cirac J I, Zoller P, Kimble H J and Mabuchi H 1997 Quantum state transfer in a quantum network: a quantum-optical implementation *J. Mod. Opt.* **44** 1727
[8] Parkins A S and Kimble H J 1999 Quantum state transfer between motion and light *J. Opt.* B **1** 496
[9] Matsukevich D N and Kuzmich A 2004 Quantum state transfer between matter and light *Science* **306** 663
[10] Wang Y D and Clerk A A 2012 Using interference for high fidelity quantum state transfer in optomechanics *Phys. Rev. Lett.* **108** 153603
[11] Blatt R and Wineland D 2008 Entangled states of trapped atomic ions *Nature* **453** 1008
[12] Stute A, Casabone B, Brandstätter B, Friebe K, Northup T E and Blatt R 2013 Quantum-state transfer from an ion to a photon *Nat. Photon.* **7** 219
[13] Christandl M, Datta N, Ekert A and Landahl A J 2004 Perfect state transfer in quantum spin networks *Phys. Rev. Lett.* **92** 187902
[14] Song Z and Sun C P 2005 Quantum information storage and state transfer based on spin systems *Low Temp. Phys.* **31** 686
[15] Bose S 2007 Quantum communication through spin chain dynamics: an introductory overview *Contemp. Phys.* **48** 13
[16] Yao N Y, Jiang L, Gorshkov A V, Gong Z X, Zhai A, Duan L M and Lukin M D 2011 Robust quantum state transfer in random unpolarized spin chains *Phys. Rev. Lett.* **106** 040505
[17] Yang W L, Yin Z Q, Xu Z Y, Feng M and Oh C H 2011 Quantum dynamics and quantum state transfer between separated nitrogen-vacancy centers embedded in photonic crystal cavities *Phys. Rev.* A **84** 043849
[18] Chen Q, Yang W L and Feng M 2012 Controllable quantum state transfer and entanglement generation between distant nitrogen-vacancy-center ensembles coupled to superconducting flux qubits *Phys. Rev.* A **86** 022327
[19] Su W P, Schrieffer J R and Heeger A J 1979 Solitons in polyacetylene *Phys. Rev. Lett.* **42** 1698
[20] Su W P, Schrieffer J R and Heeger A J 1983 Soliton excitations in polyacetylene *Phys. Rev.* B **22** 2099
[21] Hasan M Z and Kane C L 2010 Colloquium: topological insulators *Rev. Mod. Phys.* **82** 3045
[22] Qi X L and Zhang S C 2011 Topological insulators and superconductors *Rev. Mod. Phys.* **83** 1057
[23] Wu Q, Du L and Sacksteder V E IV 2013 Robust topological insulator conduction under strong boundary disorder *Phys. Rev.* B **88** 045429
[24] Chen L, Wang Z F and Liu F 2013 Robustness of two-dimensional topological insulator states in bilayer bismuth against strain and electrical field *Phys. Rev.* B **87** 235420
[25] Mei F, Chen G, Tian L, Zhu S L and Jia S 2018 Robust quantum state transfer via topological edge states in superconducting qubit chains *Phys. Rev.* A **98** 012331
[26] Palaiodimopoulos N E, Brouzos I, Diakonos F K and Theocharis G 2021 Fast and robust quantum state transfer via a topological chain *Phys. Rev.* A **103** 052409
[27] Huang L, Tan Z, Zhong H and Zhu B 2022 Fast and robust quantum state transfer assisted by zero-energy interface states in a splicing Su-Schrieffer-Heeger chain *Phys. Rev.* A **106** 022419
[28] Longhi S, Giorgi G L and Zambrini R 2019 Landau-zener topological quantum state transfer *Adv. Quantum Technol.* **2** 1800090
[29] Zheng L N, Qi L, Cheng L Y, Wang H F and Zhang S 2020 Defect-induced controllable quantum state transfer via a topologically protected channel in a flux qubit chain *Phys. Rev.* A **102** 012606

[30] D'Angelis F M, Pinheiro F A, Guéry-Odelin D, Longhi S and Impens F 2020 Fast and robust quantum state transfer in a topological Su-Schrieffer-Heeger chain with next-to-nearest-neighbor interactions *Phys. Rev. Res.* **2** 033475
[31] Qi L, Wang G L, Liu S, Zhang S and Wang H F 2020 Engineering the topological state transfer and topological beam splitter in an even-sized Su-Schrieffer-Heeger chain *Phys. Rev.* A **102** 022404
[32] Qi L, Yan Y, Xing Y, Zhao X D, Liu S, Cui W X, Han X, Zhang S and Wang H F 2021 Topological router induced via long-range hopping in a Su-Schrieffer-Heeger chain *Phys. Rev. Res.* **3** 023037
[33] Zheng L N, Yi X and Wang H F 2022 Engineering a phase-robust topological router in a dimerized superconducting-circuit lattice with long-range hopping and chiral symmetry *Phys. Rev. Appl.* **18** 054037
[34] Tzortzakakis A F, Katsaris A, Palaiodimopoulos N E, Kalozoumis P A, Theocharis G, Diakonos F K and Petrosyan D 2022 Topological edge states of the $\mathcal{PT}$-symmetric Su-Schrieffer-Heeger model: an effective two-state description *Phys. Rev.* A **106** 023513
[35] Wang C, Li L, Gong J and Liu Y 2022 Arbitrary entangled state transfer via a topological qubit chain *Phys. Rev.* A **106** 052411
[36] Bayat A, Bose S and Sodano P 2010 Entanglement routers using macroscopic singlets *Phys. Rev. Lett.* **105** 187204
[37] Pemberton-Ross P J and Kay A 2011 Perfect quantum routing in regular spin networks *Phys. Rev. Lett.* **106** 020503
[38] Paganelli S, Lorenzo S, Apollaro T J G, Plastina F and Giorgi G L 2013 Routing quantum information in spin chains *Phys. Rev.* A **87** 062309
[39] Moradi M and Karimipour V 2019 Generation of quantum states by the dynamics of spin chains: analytical solution *Phys. Rev.* A **99** 052115
[40] Yousefjani R and Bayat A 2020 Simultaneous multiple-user quantum communication across a spin-chain channel *Phys. Rev.* A **102** 012418
[41] Yousefjani R and Bayat A 2021 Parallel entangling gate operations and two-way quantum communication in spin chains *Quantum* **5** 460
[42] Lorenzo S, Apollaro T J G, Sindona A and Plastina F 2013 Quantum-state transfer via resonant tunneling through local-field-induced barriers *Phys. Rev.* A **87** 042313
[43] Kay A 2011 Basics of perfect communication through quantum networks *Phys. Rev.* A **84** 022337
[44] Li J L, Shan C J and Zhao F 2018 Exploring photonic topological insulator states in a circuit-QED lattice *Laser Phys. Lett.* **15** 045206
[45] Mei F, You J B, Nie W, Fazio R, Zhu S L and Kwek L C 2015 Simulation and detection of photonic Chern insulators in a one-dimensional circuit-QED lattice *Phys. Rev.* A **92** 041805(R)
[46] Lu L, Joannopoulos J D and Soljačić M 2014 Topological photonics *Nat. Photon.* **8** 821
[47] Yao N Y, Laumann C R, Gorshkov A V, Weimer H, Jiang L, Cirac J I, Zoller P and Lukin M D 2013 Topologically protected quantum state transfer in a chiral spin liquid *Nat. Commun.* **4** 1585
[48] Geller M R, Donate E, Chen Y, Fang M T, Leung N, Neill C, Roushan P and Martinis J M 2015 Tunable coupler for superconducting Xmon qubits: perturbative nonlinear model *Phys. Rev.* A **92** 012320
[49] Han J X, Wu J L, Wang Y, Xia Y, Jiang Y Y and Song J 2021 Large-scale Greenberger-Horne-Zeilinger states through a topologically protected zero-energy mode in a superconducting qutrit-resonator chain *Phys. Rev.* A **103** 032402
[50] DiCarlo L *et al* 2009 Demonstration of two-qubit algorithms with a superconducting quantum processor *Nature* **460** 240
[51] Mundada P, Zhang G, Hazard T and Houck A 2019 Suppression of qubit crosstalk in a tunable coupling superconducting circuit *Phys. Rev. Appl.* **12** 054023
[52] Schmidt S and Koch J 2013 Circuit QED lattices: towards quantum simulation with superconducting circuits *Ann. Phys.* **525** 395
[53] Reagor M *et al* 2016 Quantum memory with millisecond coherence in circuit QED *Phys. Rev.* B **94** 014506
[54] Reagor M *et al* 2013 Reaching 10 ms single photon lifetimes for superconducting aluminum cavities *Appl. Phys. Lett.* **102** 192604